Stochastic Versus Deterministic Variability in Simple Neuronal Circuits: I. Monosynaptic Spinal Cord Reflexes

Taeun Chang,* Steven J. Schiff,* Tim Sauer,‡ Jean-Pierre Gossard,§ and Robert E. Burke§

*Department of Neurosurgery, Children's National Medical Center, Washington, D.C. 20010; ‡Department of Mathematics, George Mason University, Fairfax, Virginia 22030; and §Laboratory of Neural Control, National Institutes of Health, National Institute of Neurological Diseases and Stroke, Bethesda, Maryland 20892 USA

ABSTRACT Long time series of monosynaptic Ia-afferent to alpha-motoneuron reflexes were recorded in the L7 or S1 ventral roots in the cat. Time series were collected before and after spinalization at T13 during constant amplitude stimulations of group Ia muscle afferents in the triceps surae muscle nerves. Using autocorrelation to analyze the linear correlation in the time series demonstrated oscillations in the decerebrate state (4/4) that were eliminated after spinalization (5/5). Three tests for determinism were applied to these series: 1) local flow, 2) local dispersion, and 3) nonlinear prediction. These algorithms were validated with time series generated from known deterministic equations. For each experimental and theoretical time series used, matched time-series of stochastic surrogate data were generated to serve as mathematical and statistical controls. Two of the time series collected in the decerebrate state (2/4) demonstrated evidence for deterministic structure. This structure could not be accounted for by the autocorrelation in the data, and was abolished following spinalization. None of the time series collected in the spinalized state (0/5) demonstrated evidence of determinism. Although monosynaptic reflex variability is generally stochastic in the spinalized state, this simple driven system may display deterministic behavior in the decerebrate state.

INTRODUCTION

The recognition that stretch reflexes are extremely variable is as old as the study of neurophysiology (Sherrington 1906). Rall and Hunt (1956) differentiated a linearly correlated from an uncorrelated component of this variability for monosynaptic reflexes. Some efforts have been made to study the covariance of these reflexes at neighboring spinal cord segments in decerebrate versus high spinal preparations (Somjen and Heath 1966). Further work (Rudomin and Dutton 1969) demonstrated that at least a portion of this variability and its correlated component may derive from the effects of presynaptic inhibition. Dual intracellular recordings of the time course of membrane potential fluctuations recorded at baseline and during excitatory postsynaptic potentials (EPSPs) were consistent with a strong correlating presynaptic effect (Rudomin et al. 1975). Correlated modulation of such variability was postulated to have an important role in the information processing of simple monosynaptic neuronal circuits (Rudomin et al. 1975). Study of single fiber Ia EPSP fluctuations have been carried out under low (Redman and Walmsley 1983) and high (Solodkin et al. 1991) synaptic noise levels, and evidence for nonlinear interactions between synaptic noise and EPSPs have been suggested (Solodkin et al. 1991).

All of the above studies assumed that the fluctuations were stochastic (random). We will here examine whether such fluctuations in monosynaptic reflex variability may in fact not be entirely stochastic, but display evidence for determinism (predictability). Many neuronal circuits in the brain and spinal cord can exhibit predictable (i.e., deterministic) behavior, such as rhythmic output under some conditions, that are easily detected by traditional linear signal analysis (power spectrum or autocorrelation). The present work was designed to test whether there are additional, more subtle, deterministic patterns in the neural output (e.g., aperiodic fluctuations in synaptic drive that nevertheless exhibit predictability) that are not revealed by conventional signal analysis. Although the basic monosynaptic reflex arc from group Ia afferents to motoneurons is a simple circuit, it is embedded in a complex system of other networks that subject Ia afferent terminals and their postsynaptic motoneurons to varying drive that may include deterministic as well as stochastic characteristics.

Many "noisy" physical systems have recently yielded unexpected patterns and insight when powerful new methods of analyzing complex systems have been applied to them. Specifically, our ability to differentiate true randomness or stochastic behavior from the highly erratic but deterministic behavior of nonlinear chaotic systems is now vastly improved (Ott 1993). Our goal in the present work was to apply these new methods to analyze the variability in neuronal population responses. In this paper we give the background and theory for these methods, and examine monosynaptic spinal cord reflexes in both the decerebrate and spinalized state. In a companion paper we examine both driven and spontaneous activity in the in vitro hippocampal slice.

Received for publication 2 March 1994 and in final form 28 April 1994.

Address reprint requests to Steven J. Schiff, M.D., Ph.D., Department of Neurosurgery, Children's National Medical Center, 111 Michigan Avenue, N.W., Washington, D.C. 20010. Tel.: 202-884-3020; Fax: 202-884-3091.

0006-3495/94/08/671/13 $2.00

MATERIALS AND METHODS

Experimental preparation

The methods used in these experiments are fully described elsewhere (Gossard et al. 1994). Four cats of unselected sex were anesthetized with halothane and the carotid arteries ligated. A tracheostomy was performed

and a catheter inserted into one carotid artery to measure blood pressure. Saline was administered through an intravenous line in a forelimb cephalic vein, and norepinephrine used as needed to keep blood pressure within physiological limits (> 80 mmHg systolic). A rectal temperature probe was used to monitor temperature, and both a heating blanket and infra-red lamp used to maintain body temperature at 37°C. A laminectomy was performed over the lumbar region to expose the cauda equina and the conus medullaris. The muscles of the left leg were extensively denervated and the nerves to the medial gastrocnemius, lateral gastrocnemius, and posterior biceps and semitendinosus muscles were placed on fine platinum bipolar electrodes for stimulation. After craniotomy, the forebrain was removed and a precollicular transection of the midbrain was performed. A laminectomy was performed at T13 to permit later spinalization. The animals were paralyzed with gallamine triethiodide (Flaxedil), and the proximal ends of the cut ventral roots of L7 and S1 were placed on bipolar platinum recording electrodes. The spinal cord and roots were immersed in warmed mineral oil.

Constant voltage 50 μsec square-wave stimuli were applied to single muscle nerves in the lower extremities at a frequency of 2 Hz. The intensity of stimulation was adjusted to yield just supra-maximal group I responses as measured by the cord dorsum potential (recorded with a fine platinum ball placed on the dorsal root entry zone). We attempted to evoke monosynaptic reflexes with single stimulus volleys delivered to medial gastrocnemius, lateral gastrocnemius and soleus, or to posterior biceps-semitendinosus muscle nerves (Table 1). However, for some of the experiments it was necessary to use two stimulus volleys to evoke a measurable monosynaptic reflex (4 msec interval between paired volleys, pairs delivered at 2 Hz); special attention was given in these cases to eliminate reflex series showing any detectable response to the first volley. In the spinalized phase of experiment 1, time series in response to single pulse stimulation of both medial gastrocnemius and posterior biceps-semitendinosus nerves were available and analyzed (Table 1); the spinalized data therefore reflect 5 data sets from 4 experiments, and are not statistically independent.

Recordings were stored digitally and analyzed with LabView2 (National Instruments, Inc., Austin, TX), or Datapac II (Run Technologies, Inc., Laguna Hills, CA). Implementation of algorithms to test for determinism was performed with Matlab (The Math Works, Inc., Natick, MA).

In the analysis of these data, time window settings were set to incorporate the positive deflection of the monosynaptic reflex potential (Figure 1). These recordings were made from "crushed-end" ventral roots in order to remove biphasic and triphasic components. Baseline potential recordings just before the monosynaptic reflex were subtracted to give the absolute voltages recorded at the time of the reflex, and the monosynaptic reflex deflections were integrated during a time window of 1–2 msec. Previous work suggests that this integrated value is proportional to the number of discharging neurons in the motoneuron pool (Rall 1955).

TABLE 1 Summary of experiments

Experiment	Events	Preparation	Roots	Pulse*
1A	2455	Decerebrate	MG/LGS	1
1B	1018	Spinal	PBST	1
1C	1118	Spinal	MG	1
2A	536	Decerebrate	MG/LGS	2
2B	825	Spinal	MG/LGS	1
3A	970	Decerebrate	MG/LGS	2
3B	1000	Spinal	MG/LGS	2
4A	623	Decerebrate	MG/LGS	1
4B	1000	Spinal	MG/LGS	2

MG, medial gastrocnemius; LGS, lateral gastrocnemius and soleus; PBST, posterior biceps—semitendinosus.

* Whether the monosynaptic reflex integrated was in response to the first or second stimulation pulse. Second pulses were used if a pair of stimuli were required to evoke a monosynaptic reflex, and there were no responses to the first pulse in any trial (see Gossard et al., 1994).

Mathematical background

Some very simple systems have extremely complex behaviors. Simple models of fluid convection (Lorenz 1963) revealed that atmospheric gases may behave in a complex fashion, explaining in part why weather forecasting is so imprecise. May (1976) demonstrated how a very simple model of insect populations may give extraordinarily complicated yearly population measurements. These two theoretical models derived from simple nonlinear equations (where, for instance, a variable was "squared"), and were fully deterministic.

Unfortunately, the experimental scientist usually has no access to the actual underlying equations (rules) that generate the behaviors of an observed system. The experimentalist measures one or more observable variables, and is then faced with the task of modeling the underlying true system. For the two examples mentioned above, simple study of the statistical properties in time, or in frequency (e.g. Fourier analysis), is poorly equipped to give much insight into the underlying dynamics. As a result, a method to reconstruct the dynamics of such a system has been developed - time delay embedding.

Time delay embedding

A physical system that follows a well described set of rules (e.g. differential equations) may be represented by a graph in a "state" space, where each coordinate represents an independent variable of the system. Thus, the state of a rolling marble may be described by a plot of its position and momentum, or a swinging pendulum may be represented by a plot of its angle and angular velocity. For dynamical systems whose true variables are unknown, we can observe one physical measurement over time, creating an experimental time series. In time delay embedding, one creates additional variables (coordinates) by using previous (delayed) measurements of the time series, and plots a trajectory in a vector space that we hope will capture some of the characteristics of the original system's trajectory in its true state space. We hope that the number of coordinates we require to represent the dynamics of the original system in our reconstructed state space correspond well to the number of variables (degrees of freedom) present in the true system. In this study, we will use the term *embedding dimension* to specify the number of time delay coordinates we are using. It is important to note that high dimensional systems, even when very deterministic, will appear stochastic by these methods.The physics of time delay embedding was first explored by Packard et al (1980) and Takens (1981), while the mathematical foundation extends back to Whitney (1936). An accessible discussion of the experimental applications of this technique can be found in Moon (1992). A detailed theoretical analysis of this method is given by Sauer et al (1991).

Determinism

Determinism implies that the trajectory of the state of our system has predictability—that there are rules that direct, at least to some degree, the direction and magnitude of the evolution of the trajectory from any given coordinate. Completely deterministic systems, which are unexpected experimentally in biological systems, would have fixed rules for knowing exactly where the system's state variable will move given an initial set of coordinates. A perfect reconstruction of these dynamics from delay coordinate embedding would enable us to predict the true system's trajectory well. Unfortunately, we anticipate that if biological systems exhibit deterministic dynamics, our measurements will reflect mixtures of dynamical and additive noise blended with the deterministic elements. This noise will degrade the quality of our reconstructed map, and although this will increase the error in our predictions, our short-term accuracy may still be good. *A "good" prediction is better than a random choice.* To test the effectiveness of prediction, we will compare our predictions with known random choices. We will do this by constructing families of randomized data based on the original observations, called "surrogate data". We then test the surrogate sets to see how well these control data sets can account for our experimental predictions.

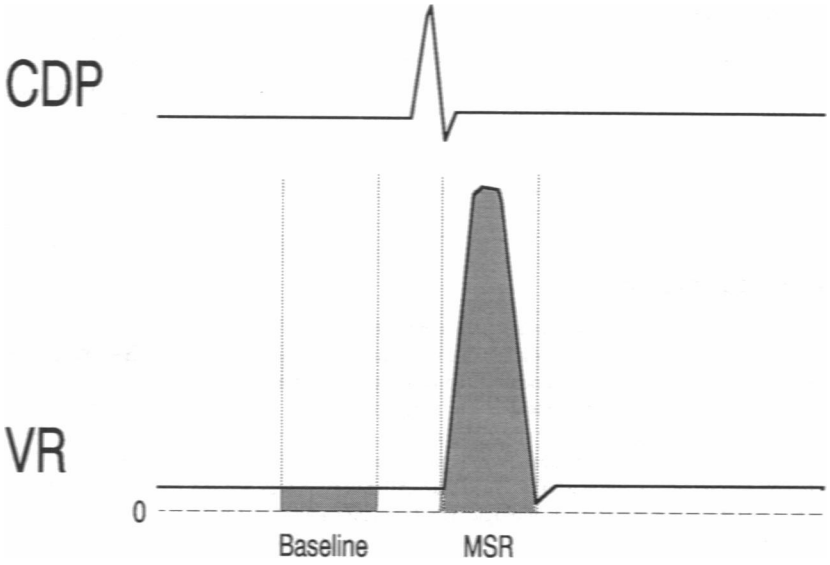

FIGURE 1 Scheme for data analysis from electrical recordings. Upper trace shows cord dorsum potential (CDP) in relation to monosynaptic reflex (MSR) from ventral root (VR) "crushed end." Crushing the end of the root, where it rests on one of the bipolar electrode leads, reduces the triphasic components of the MSR to a nearly monophasic potential that is readily integrated without rectification. A section of integrated VR baseline, equal in time span to the MSR window used for the integration boundaries, is subtracted from the integrated MSR to ensure accurate integrations in the face of baseline drift.

Local smoothness

Unfortunately, our imperfect trajectory map will fail us if the trajectories for nearby coordinates are wildly different. When we observe this, the system will appear stochastic. We therefore need to hope that there is some local "smoothness" to our rules—i.e., that the rules for neighboring points are similar. A local smoothness assumption underlies each of the methods we will employ to test for determinism in this study. Local smoothness, of course, is also a characteristic of stochastic systems that possess linear correlation; we therefore employ surrogate data with degrees of local smoothness that are similar to our experimental data in order to take this into account.

Linear systems may of course be predictable, and methods for describing time series prediction of such systems are well described (Box and Jenkins 1976). Such systems are well characterized by their component frequencies (power spectrum) or linear correlation (autocorrelation), measurements of which offer an equivalent and complete description of linear systems (Bendat and Piersol, 1986). ***In the present work, we will attempt to identify predictability beyond that accounted for by the spectrum, and this is the hallmark of nonlinear and potentially chaotic systems.*** Such systems may be deterministic, yet display irregular and aperiodic behavior that can be mistaken for "noise."

Tests for determinism

Three independent tests for determinism were used in this study because we have no a priori knowledge regarding which of these methods are best to use with these types of biological data. As opposed to examining the original data in time (autocorrelation), or in frequency (Fourier analysis), these methods examine the behavior of nearby points in the time embedded vector space. All of these methods deal with patterns of flow of nearby points in this vector space (one thinks of local eddy currents in turbulent fluid, where on a small scale nearby fluid *flows* together). Since the mathematics of these methods are complex, we have placed all equations in an Appendix. Source code for the implementation of each method may be found in Schiff et al (1994).

Local flow

We begin with the time delay embedded representation of the data (not the original data; see Appendix A1). Our first method to test for determinism is a discrete adaptation (Kaplan 1993) of a technique for continuous systems (Kaplan and Glass 1992). In the discrete adaptation of this method (Figure 2A), one first selects points in the embedding space that are "nearby". Using these as reference points, vectors are calculated to events in the embedding space at a selected time in the future. We denote the time translation selected for these points as the *translation horizon*. These vectors are then normalized and averaged. Larger average vectors are produced by deterministic rather than stochastic systems. Although deterministic structure might be observed for small translation horizons, evidence for determinism will generally be lost as the translation horizon is increased.

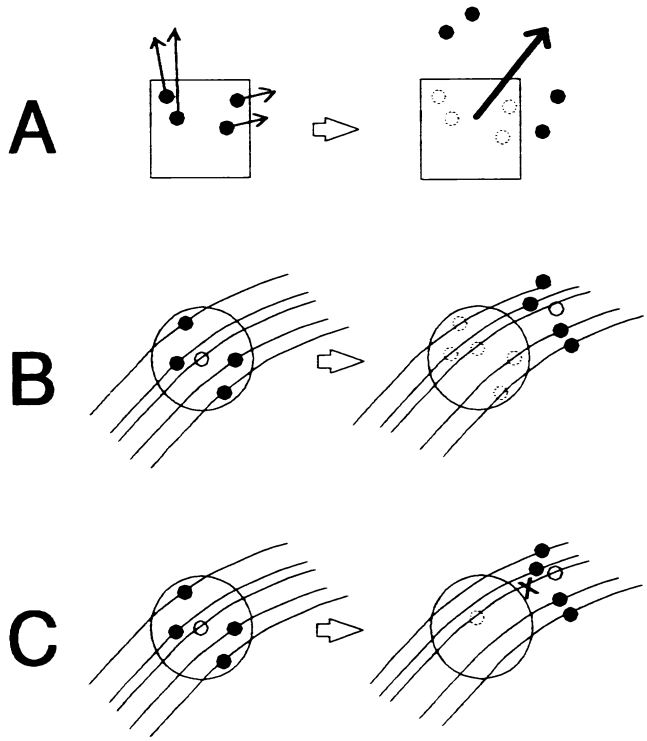

FIGURE 2 Geometry of the mathematics employed in the three tests for determinism. (*A*) Local flow; (*B*) local dispersion; (*C*) nonlinear prediction. (●) Position of the points in the embedding space, near a given index point indicated by (○). Dashed open circles indicate the original positions of index points, before translated into the future for a given translation horizon. The X is a predicted location for nonlinear prediction (*C*).

Local dispersion

A closely related method to test for determinism examines the consistency with which nearby points (in the embedding space) move with time (Wayland et al. 1993; see Appendix A2). If nearby points all tend to move relatively similar distances in similar directions, that is the variance or dispersion of the nearby movements is small, this is evidence for determinism (Figure 2B). If the movements are widely dispersed, the process may be stochastic.

Nonlinear prediction

For our third method, we choose index points in the embedding space, and study how the neighbors of those points move with time (see Appendix A3). We take an average of the movement of the neighbors, and compare this prediction with the actual movement of our index points. The difference between the actual and predicted movement is the error of our prediction (Figure 2C). This type of nonlinear prediction technique was explored in detail by Farmer and Sidorowich (1988), and a similar version was applied to the dynamics of measles epidemiologic data (Sugihara and May 1990). To make our analysis as transparent as possible, we employed a relatively simple implementation of this technique, although more elaborate implementations exist (Sauer, 1993).

Autocorrelation

Autocorrelation is a function that is a measure of the linear correlation present in a time series (Box and Jenkins 1976). This function calculates the correlation between points in a time series at various time "lags" (see Appendix A4).

Surrogate data

We have constructed statistical controls from our experimental data to test the null hypothesis that our results can be explained by non-deterministic processes. We in particular want to exclude predictability in our data that can be well accounted for by linear correlation in time. We have used the method of surrogate data, where certain aspects of the data are preserved (e.g. number of data points, mean, standard deviation, autocorrelation), yet the data are randomized to destroy deterministic structure that may be present. If the results of the experimental and surrogate data are similar, then we cannot reject the null hypothesis that our data are stochastic (for review, see Theiler et al. 1992).

For each of our experimental time series, we have constructed 3 separate realizations of each type of surrogate data set, and analyzed them in the same manner as our experimental data. One then tests to see if the experimental data yields results outside of the distribution of the surrogate data results.

The source code for generating these different surrogates can be found in Schiff et al. (1994).

These surrogates are not the only possibilities. Kaplan and Glass (1993) have recently demonstrated how creatively constructing surrogates can help reduce spurious conclusions from stochastic data.

Our use of surrogate data also provides a safeguard against generating spurious results due to small data set size. Indeed, we would have preferred to have very long data sets for these analyses, but the nature of the biological systems employed limited us. Nevertheless, by matching the size of the surrogates to the size of the data sets, artifacts related to data set size should be accounted for.

It is important to note that our surrogate data sets are actually linear stochastic models of the data. By comparing the surrogate with experimental results in our tests for determinism, *we are specifically seeking to identify determinism beyond that imparted by the autocorrelation, and by implication inconsistent with these linear models.*

Phase randomized surrogate

We have used three types of surrogate data. In the first type, phase randomized, we preserve the mean, standard deviation, and autocorrelation of our original time series (Theiler et al. 1992). Recall that a Fourier transform generates a sequence of complex numbers, the amplitudes of which correspond to the power spectrum, and the phases of which are essential to reconstruct the original time series through an inverse Fourier transform. A random phase can be added to each complex coefficient of a Fourier transform, and an inverse Fourier transform then generates a new random time series which has the same mean, standard deviation, and autocorrelation as the original (for further details see Appendix of Schiff 1992). Preserving autocorrelation implies that the surrogate time series has the same "smoothness" as the original time series, and therefore it has the same frequency content (power spectrum).

Gaussian scaled surrogates

The second type of surrogate is one where we assume that the data came from a normally distributed (Gaussian) random process, that was filtered through a nonlinear filter (e.g. synapses, bad amplifiers, etc). In this surrogate the original data values of the experimental time series are shuffled, which preserves the amplitude distribution of our data but not the autocorrelation (the phase randomized surrogate changes the amplitudes of the data in order to preserve autocorrelation). We call this a Gaussian scaled surrogate, and it was proposed by Theiler et al. (1992). The surrogate is created by generating a Gaussian distributed set of random deviates with the same number of points as the original time series. These random numbers are then rank ordered in the rank order of the original time series (rank order is the sequence of numbers that indicate the relative amplitudes of the

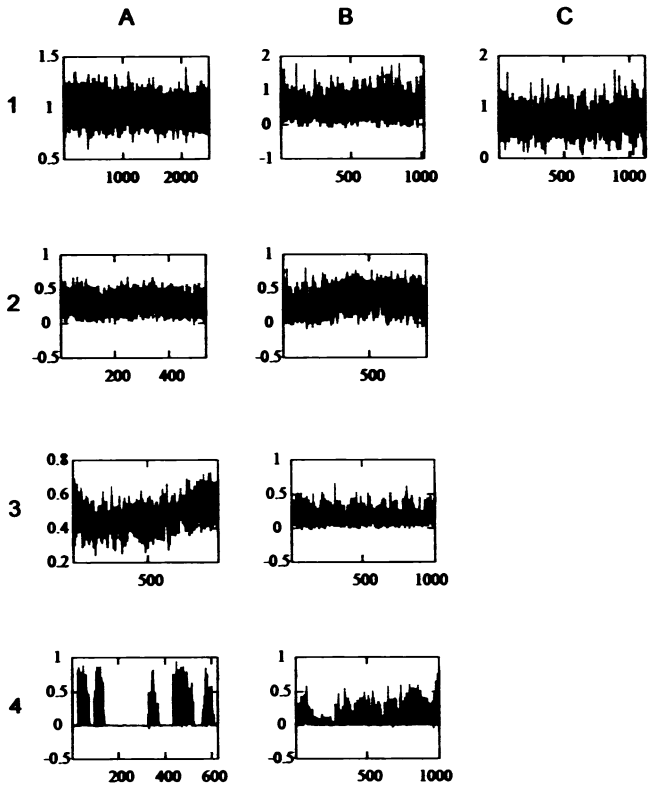

FIGURE 3 Integrated monosynaptic reflex time series from experiments 1–4. Columns *A*, *B*, and *C* correspond to different time series as detailed in Table 1. All of the data in column *A* are from decerebrate preparations, whereas columns *B* and *C* are from spinalized preparations. Two sets of spinalized data are shown from experiment 1 corresponding to different reflexes (Table 1). Note the presence of fictive walking during the decerebrate phase of experiment 4 (this time series was not convincingly deterministic). Abscissa are event numbers, each event recorded at 2 Hz. Ordinates are arbitrary values proportional to ms*mV.

elements in a time series, so that {3, 2, 5} would have a rank order of {2, 1, 3}). One then generates a phase randomized surrogate of this rank ordered sequence of random numbers, and then rank orders the original time series in the rank order of this phase randomized surrogate.

Fourier shuffled surrogate

Our third surrogate was constructed to overcome some of the difficulties encountered with the Gaussian scaled surrogates. We have constructed a surrogate, again from the original data values of our experimental time series, but have tried to approximate as closely as possible the linear correlation or smoothness as in the original data. The surrogate is created by generating a phase randomized surrogate of the original time series, and then rank ordering the original data values in the rank order of this phase randomized surrogate. We call this a Fourier shuffled surrogate.

RESULTS

Nine time series were analyzed from four experiments (Table 1). Figure 3 shows the original experimental time series of the integrated areas of the monosynaptic reflexes. Figure 4 shows the autocorrelation of each original time series. All (4/4) of the decerebrate time series demonstrated oscillations or "seasonality" in the autocorrelation. This reflects relatively slow oscillatory behavior in the autocorrelation as a function of time lag shown along the abscissas of Figure 4. In no time series collected after spinalization (0/5) was this oscillatory autocorrelation observed.

To validate the determinism algorithms we used (local flow, local dispersion, and nonlinear prediction), we have tested them with a chaotic time series generated from a known deterministic set of equations—the Hénon (1976) equations (see Appendix A5). Figure 5 shows a chaotic time series generated from observing 1 variable from the Hénon equations. This time series appears to be random noise to the observer, yet it is generated by iterating a set of deterministic equations, and the complete time series can be "predicted" (i.e. replicated) by iterating the equations *when the initial conditions are exactly specified*. Also shown in Figure 5 are three matched surrogate data sets for this time series: Fourier shuffled, phase randomized, and Gaussian scaled. Figure 6 shows the results of each method applied to the Hénon time series, and the three types of surrogate data. We have generated *three independent realizations for each of the three types of surrogate data* (with different random numbers). As can be seen, each method is readily capable of picking out

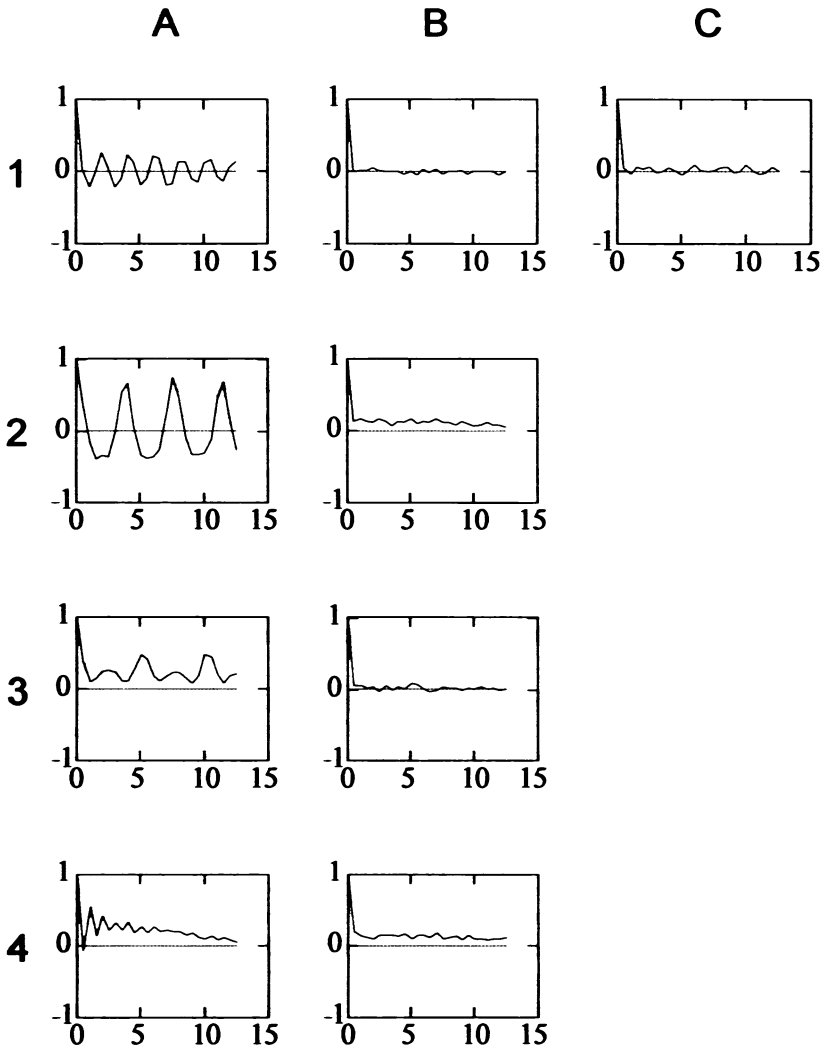

FIGURE 4 Autocorrelation for the time series shown in Fig. 3. Note the oscillatory behavior of the autocorrelation in the decerebrate preparations (column *A*), which is almost entirely eliminated in the spinalized data (columns *B* and *C*). Abscissa is time in s. Time lags in the computations were used in increments of 0.5 s.

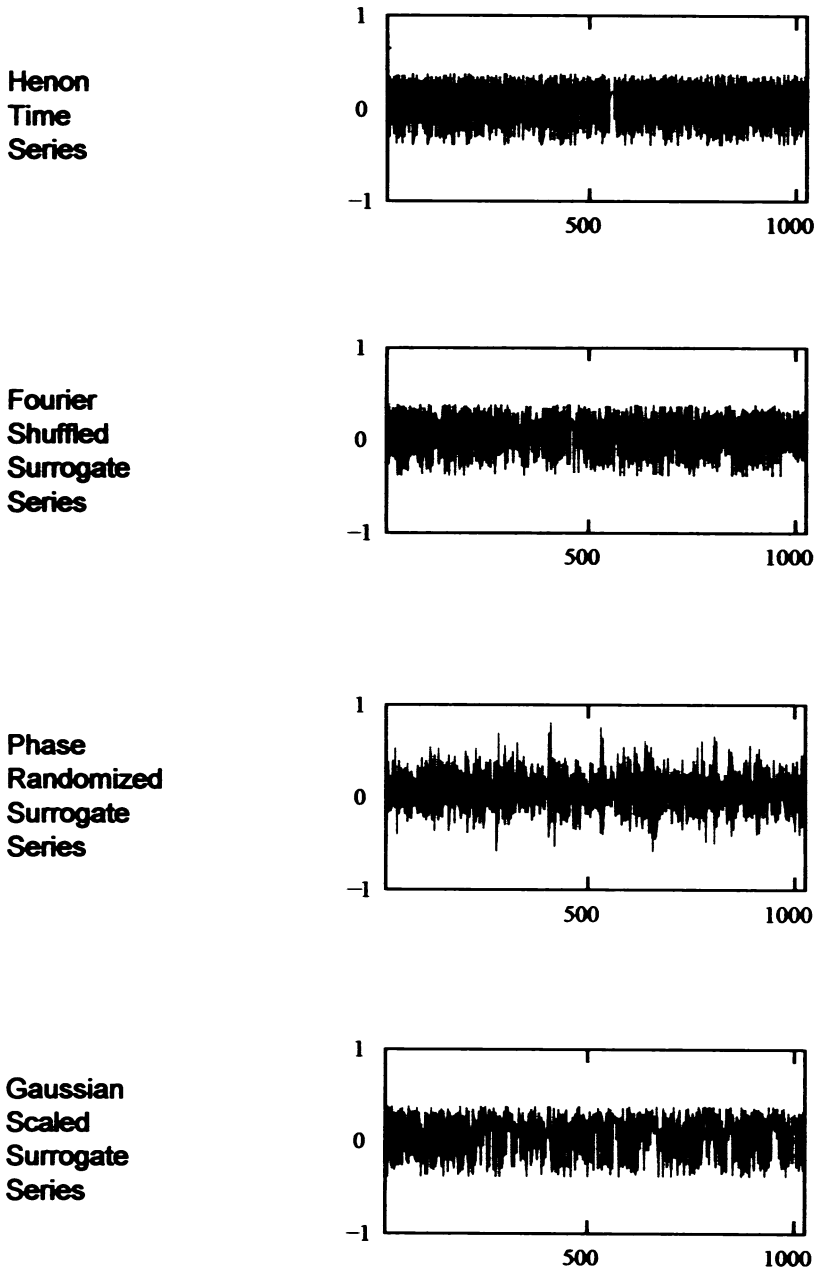

FIGURE 5 Theoretical time series data generated from the chaotic Hénon equations (see Appendix). The original time series is shown, as well as phase-randomized, Gaussian-scaled, and Fourier-shuffled surrogates. Note that the Fourier-shuffled and Gaussian-scaled surrogates preserve the original values of the time series, whereas the phase-randomized surrogate uses new values (while maintaining the autocorrelation of the original time series).

the deterministic qualities of this time series by giving different results (diamonds, Figure 6) when compared with the distribution of the surrogate data results (dashed lines, Figure 6).

To quantify these results, we use a technique suggested by Theiler et al (1992), where for each value of the experimental result plotted along the abscissa, the standard deviation for the surrogate results is calculated, and the number of standard deviations, "sigmas", separating the surrogate mean from each experimental value are determined. For the Hénon results in Figure 6, the Null hypothesis that the deterministic properties of the data can be explained with the properties of the surrogates can be rejected. We focus on the least separation between surrogate and experimental results, because if any surrogate data can fit the results well, determinism is not likely present. For local flow calculations, Fourier shuffled surrogates (the closest fit) averaged 6.4 sigmas in separation from experimental values for 10 translation horizons (translation horizon is the number of discrete time units that points are translated into the future, see Methods). For local dispersion, the closest fit averaged 13.1 sigmas in separation from experimental values over 8 embedding dimensions for Fourier shuffled surrogates. For nonlinear prediction, the closest fit averaged 29 sigmas over 10 translation horizons for Fourier shuffled surrogates.

All of the experimental time series after spinalization (5/5) failed to demonstrate evidence of determinism, suggesting that these reflexes fluctuated stochastically. The results of the local flow, local dispersion, and nonlinear prediction analysis for a typical spinalized time series, experiment 3B, are shown

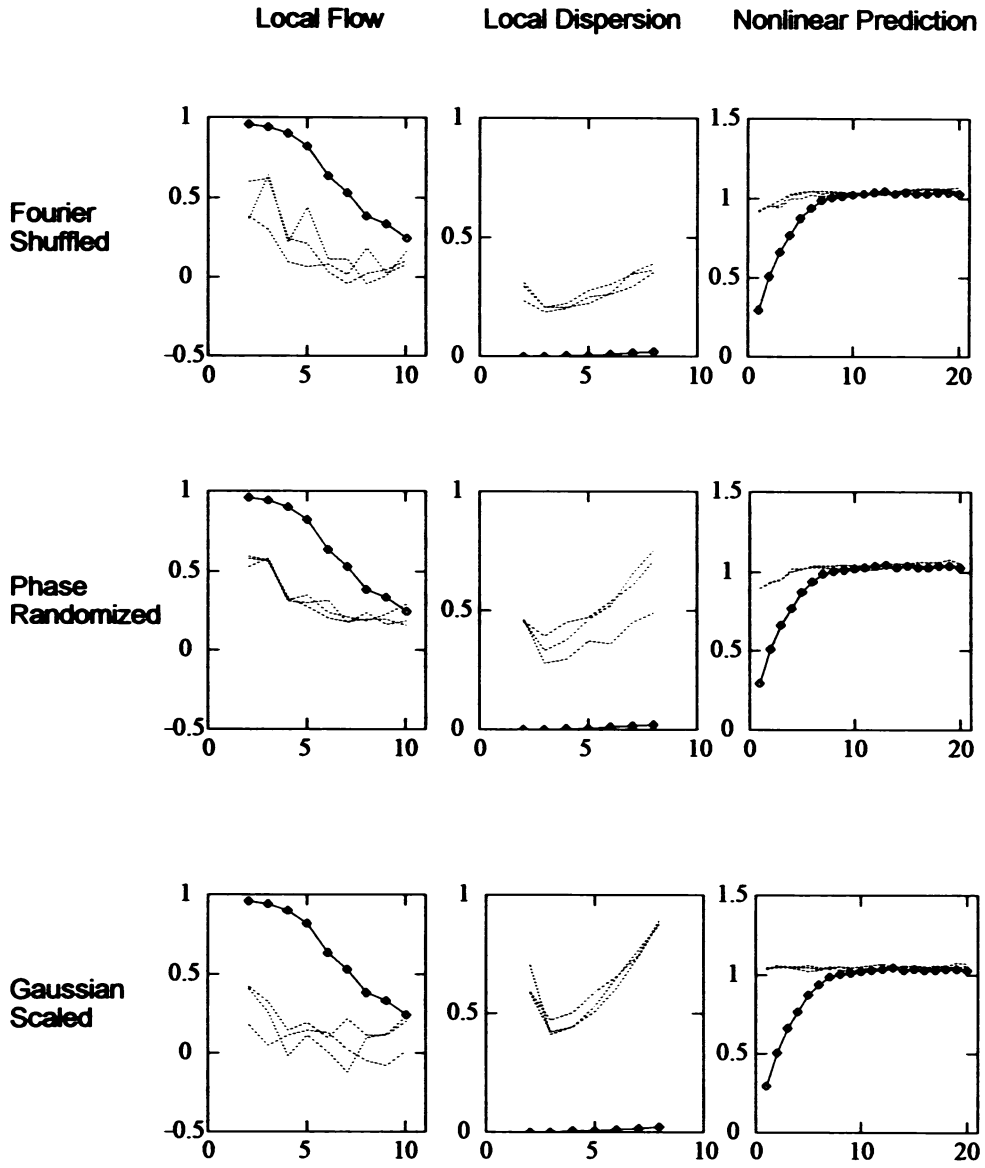

FIGURE 6 Results of local flow, local dispersion, and nonlinear prediction algorithms on the Hénon data, compared with three sets of each of the three types of surrogate data. Diamonds (◇) represent the experimental, and dashed lines (- - - -) represent the surrogate data results in this and subsequent figures. As can be seen, each method is readily capable of detecting the determinism in these data, showing clear separation from the results obtained with the surrogate data. The abscissa are translation horizons for local flow and nonlinear prediction, and embedding dimensions for local dispersion plots. Embedding dimensions are four and eight for local flow and nonlinear prediction, respectively, and local dispersion translation horizons are one in this and subsequent plots.

in Figure 7. In this example, the results of the analysis for 3 sets of different types of surrogate data matched to the original time series were indistinguishable from the original experimental data.

Half (2/4) of our decerebrate data demonstrated evidence for determinism that could not be accounted for by our surrogate controls. As in the case of the Hénon equations, not all of the methods used showed equal sensitivity in identifying determinism in these series. In data from experiment 3A, the local flow and local dispersion methods failed to identify deterministic structure, yet the nonlinear prediction method showed a detectable amount of predictability for short times with all surrogates (Figure 8). The closest fit of our surrogate data (phase randomized) still averaged 4.8 sigmas for the first 8 translation horizons for nonlinear prediction. A more dramatic example is seen in data from experiment 2A. In this time series, deterministic structure was clearly evident (Figure 9). The best surrogate fit (phase randomized) for local dispersion calculations showed a consistent separation between the surrogate and experimental data (Figure 9), averaging 2.0 sigmas of separation for the first 8 embedding dimensions. Nonlinear prediction showed clear separation between experimental data and controls, averaging 14.0 sigmas of separation for the first 20 translation horizons for the best surrogate fit (Gaussian scaled, Figure 9).

DISCUSSION

These results suggest that monosynaptic reflex variability at the group Ia to alpha-motoneuron synaptic junction may be partially deterministic in the decerebrate state. It is important to note that this determinism is over and above the effects of the obvious periodicity present in the autocorrelations illustrated in Figure 4. Our analysis was designed to separate predictability that could be explained by a simple linear process, from predictability that would require a more complex

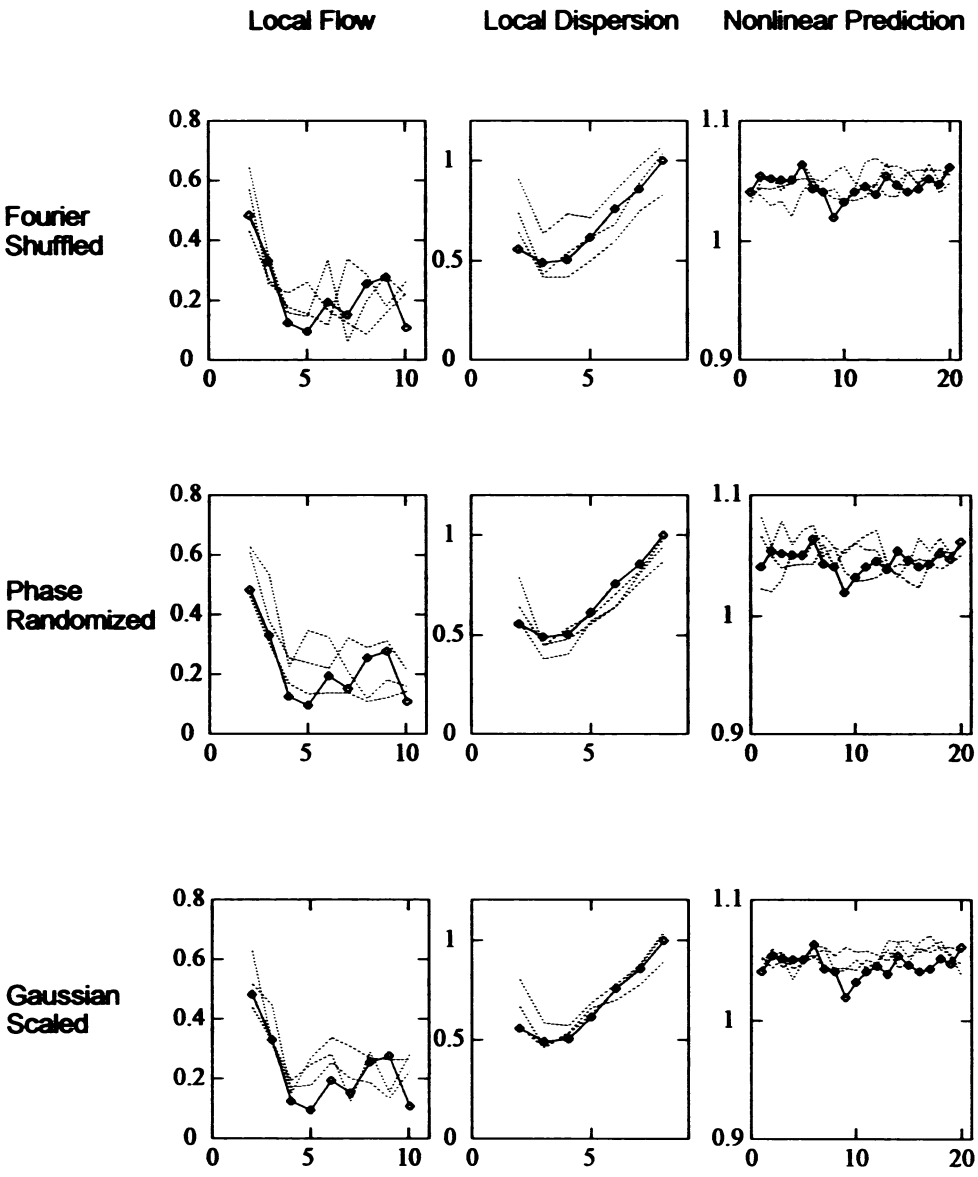

FIGURE 7 Results of local flow, local dispersion, and nonlinear prediction algorithms for data from the spinalized phase of experiment 3 *B*. No evidence for determinism is detected. Layout as in Fig. 6.

model to explain (e.g. nonlinear, perhaps chaotic). Following spinalization, both the oscillatory autocorrelation and the deterministic structure were lost.

The present work reports analyses of experimental records that were part of a broader study of the origins of monosynaptic reflex variability that is reported elsewhere (Gossard et al., 1994). The results of that study provide evidence that the variability of group Ia monosynaptic reflexes arises from both presynaptic and postsynaptic sources, with predominance of the latter. Synaptic drive from common sources, primarily spinal interneurons, onto many group Ia synaptic terminals and motoneurons of the responding motor pool are responsible for correlated fluctuations of motoneuron excitability during monosynaptic reflexes. In addition, there is evidence that some sources of postsynaptic drive to pool motoneurons are not homogeneously distributed within the motor pool. Such non-homogeneous input sources produce fluctuations of excitability only in certain subpopulations of pool motoneurons and thus are not correlated with the excitability fluctuations in the overall population response (Rall and Hunt, 1956). The available evidence suggests that some "uncorrelated" sources of variability may be randomly distributed among pool motoneurons, resulting in what can be regarded as stochastic "noise" in the population responses. However, other sources appear to affect subpopulations of sufficient size as to produce systematic changes in the identities of responding motoneurons at any given level of overall population response (Gossard et al., 1994). Intrinsic sources of variability such as fluctuations of transmitter release at individual synaptic terminations and stochastic behavior of neuronal membrane channels are inherently uncorrelated and would not be expected to produce substantial population variance, given the very large number and small magnitude of such effects. We speculate that the strong oscillatory autocorrelations observed in the decerebrate state may reflect the activity of supraspinal structures acting on the central rhythm generator of the spinal cord (Grillner 1981).

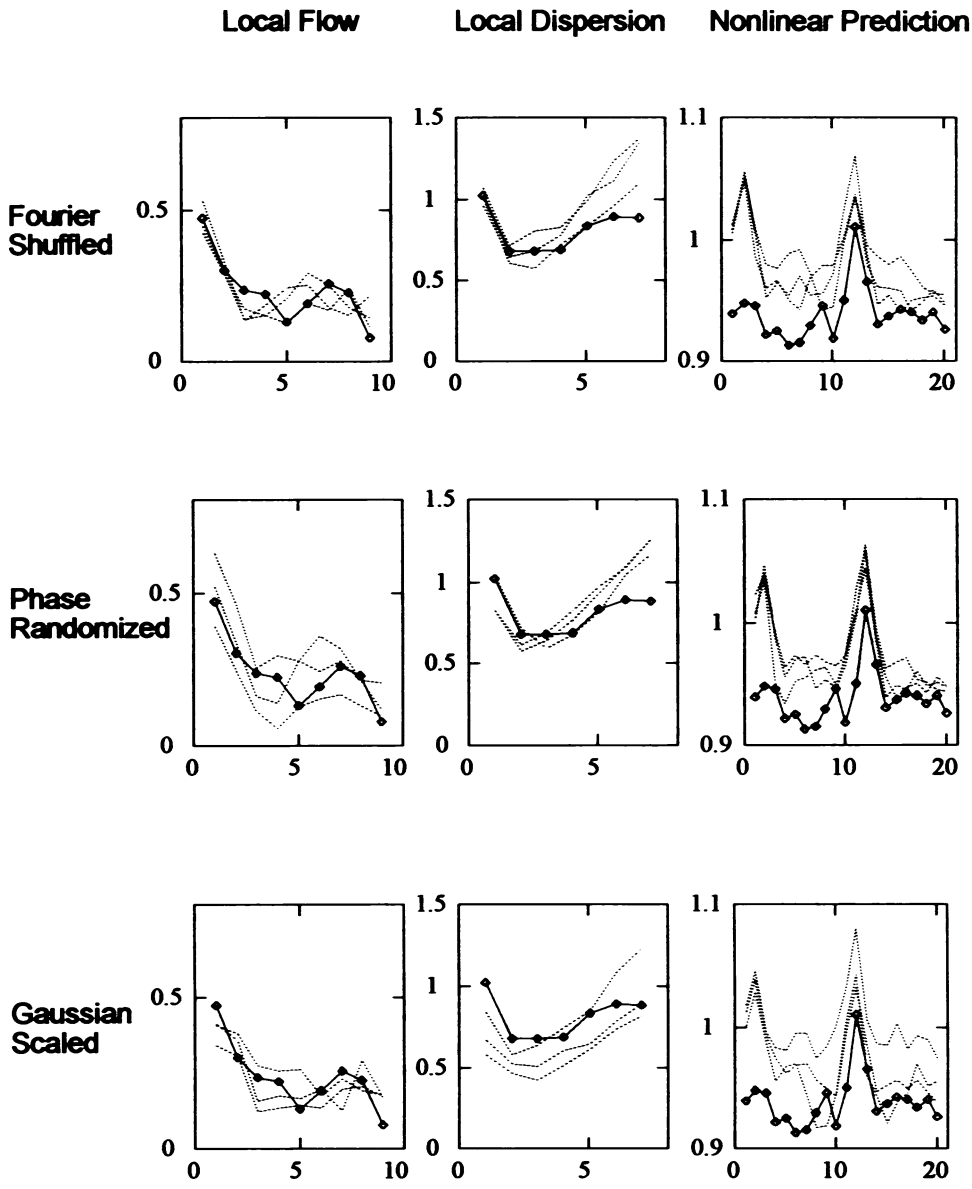

FIGURE 8 Results of local flow, local dispersion, and nonlinear prediction algorithms for data from the decerebrate phase of experiment 3*A*. Evidence for determinism is seen only for nonlinear prediction and is not apparent for the other methods.

If neuronal population information processing on an elemental level was deterministic, one would anticipate that by increasing the isolation of the reflex circuit with spinalization, the degree of determinism observed would increase. We found no evidence for this; only when the monosynaptic reflexes were incorporated into a larger scale neuronal network (decerebrate), was some degree of determinism observed.

We made no effort to adjust the amplitude of stimulation to standardize the mean values of the monosynaptic reflexes (Rudomin and Dutton 1969). For the predictability we were testing for, the surrogate data controls should have prevented spurious deterministic results due to this effect. As in previous work, we have assumed that stimulation maximal for group I fibers produces a constant level of group Ia input to the system (Rudomin et al. 1975).

We recognize that we have used a fairly low frequency of periodic stimulation to strobe our system. Dynamical behavior occurring on time scales much faster than our stimulation would be difficult to capture with our embedding method. Although one approach is to use higher rates of stimulation, there is a rapid decrease in monosynaptic reflex amplitude as frequencies approach 50 Hz (Lloyd and Wilson 1957). Nevertheless, it appears that different stimulation frequencies can effect the recruitment order of motoneurons (Gossard et al 1994), and whether such frequency effects may also alter the deterministic qualities of monosynaptic reflexes is unknown at present.

Our finding of deterministic (and presumably chaotic) structure in some, but not all, of the decerebrate preparations begs the answers to a host of questions which we are ill equipped to provide. We do not know what induced this system in half of our decerebrate preparations to display deterministic behavior. We have not attempted to estimate the apparent number of degrees of freedom present for these chaotic examples. We have used no noise reduction scheme

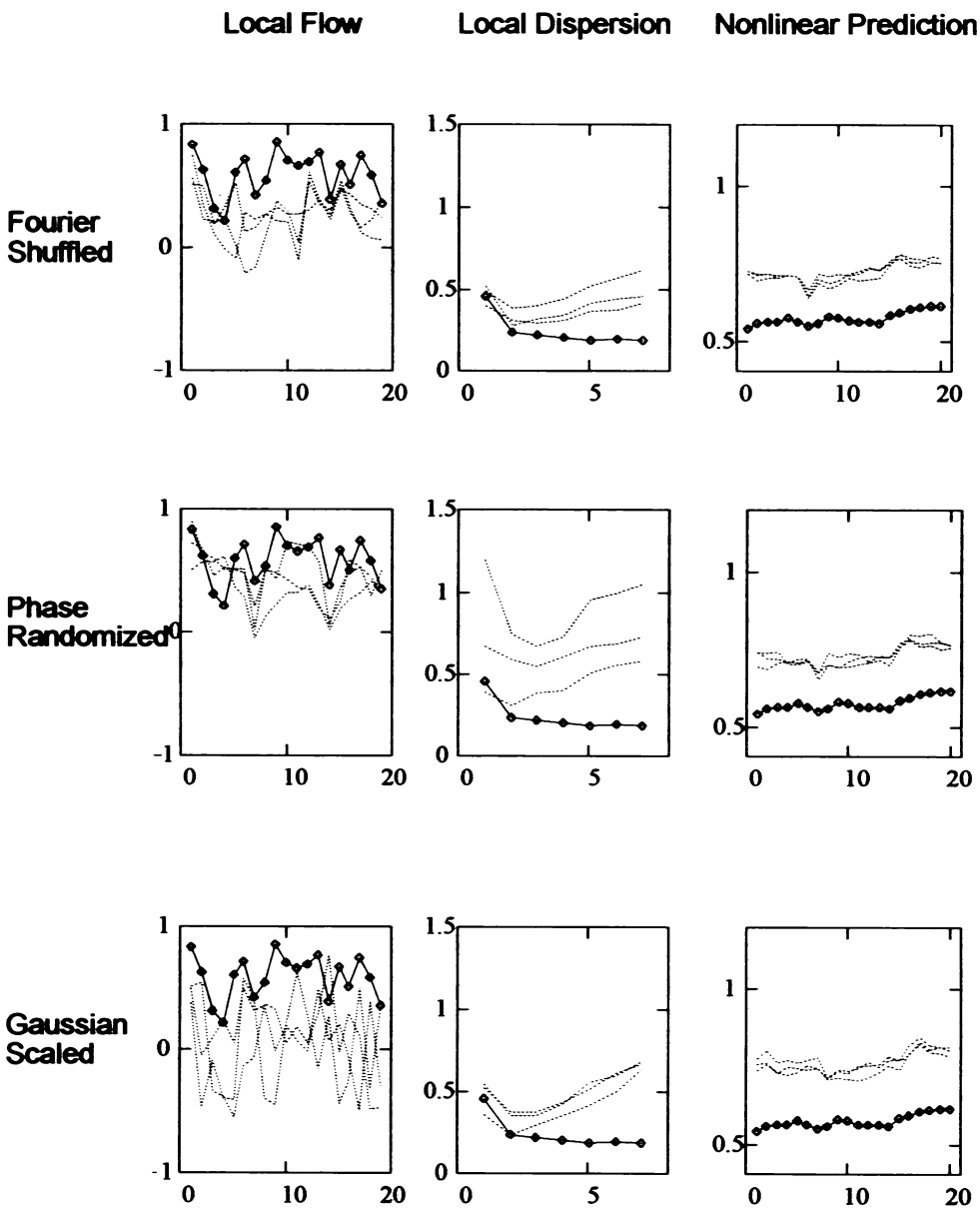

FIGURE 9 Results of local flow, local dispersion, and nonlinear prediction algorithms for data from the decerebrate phase of experiment 2A. Here, local dispersion results are weakly positive, but nonlinear prediction is strongly positive for determinism.

on these data, and it is possible that a suitable noise reduction method, especially when used on the reconstructed coordinates (Broomhead and King 1986, Kostelich and Yorke 1990, Sauer 1992), might reveal some degree of determinism in our other time series. In addition, we are aware of the possible artifacts that can be induced in an analysis such as ours from data with long coherence times (Theiler et al. 1993).

Although we have used three independent tests for determinism in this study, these tests do not appear equivalent in their sensitivity to detect determinism. We have recently completed a detailed theoretical comparison of these methods, and confirmed that the relative sensitivities implied by our results (Figures 8 and 9) can be replicated using theoretical data sets with additive noise (Chang et al. 1994). We recognize that the use of different parameters (e.g. embedding dimension) and averaging techniques employed by each method makes a direct comparison difficult. Nevertheless, such a comparison still serves to illustrate the relative power of each algorithm to pick up determinism in the presence of noise.

Two of the obvious problems in the attempted application of chaos theory to the nervous system have been the lack of mathematical controls, and the application of these ideas to excessively complex systems. Recall that the equations used to generate visually complex and attractive patterns (such as the Hénon equations), are in reality extremely simple nonlinear equations. We have attempted to deal with these issues by using the most rigorous controls available through our surrogate data sets, and by restricting our attention to one of the simplest of known mammalian neuronal circuits. Nevertheless, our analysis relied upon relatively few surrogate trials, and the assumption that their distribution was Gaussian. Our statistics would have been improved by using ad-

ditional surrogates, but the computational demands rapidly become excessive.

There are known clinical correlations for reflex variability. In the modern form of spasticity surgery known as selective dorsal rhizotomy, reflex measurements are employed in order to select dorsal rootlets for section. It has recently been shown that reflex variability affects the performance of such surgery (Weiss and Schiff 1993), and further clarification of this issue has recently been provided using an animal model (Rivera et al. 1994). Unfortunately, the reflex measurements made during clinical spasticity surgery are polysynaptic, and the data both sparse and contaminated by measurement noise (see, e.g., Weiss and Schiff 1993). The type of analysis performed here on monosynaptic reflexes recorded in a laboratory setting may reveal processes that underlie clinical phenomena, but making direct correlations between these laboratory and clinical findings would be inappropriate at this time.

There are several reasons why finding evidence of determinism in neuronal circuits such as this is important. Foremost is that whether these circuits operate stochastically or deterministically must be a fundamental feature of any model that can explain how this region of the central nervous system actually processes information. In addition, a realistic model must take into account under what conditions such neuronal circuits might switch between stochastic and deterministic behavior.

Another issue is control. With the theoretical prediction that chaotic physical systems might be readily controllable with small perturbations (Ott et al. 1990; Shinbrot et al. 1993), there has been rapid and successful application of this technique to mechanical systems (Ditto et al. 1990), lasers (Roy et al. 1992), and cardiac tissue (Garfinkel et al. 1992). What is predictable is in principle controllable. Whether the nervous system uses some variant of these methods to control simple fluctuating neuronal circuits, or whether one might intervene experimentally to effect a degree of control over such circuitry, are both intriguing speculations.

We are grateful to J. Theiler and D. Kaplan for their helpful discussions. Portions of this work were supported by grants to S. J. Schiff from the American Paralysis Association (contract #SB1-9202-1) and National Institutes of Health (1 R29 MH50006-01), and support from the Children's Research Institute. T. Chang received support from the Children's Research Institute. T. Sauer was partially supported by the National Science Foundation Computational Mathematics program and the Department of Energy. J.-P. Gossard was supported by a Centennial bursary from the Medical research council of Canada. The contribution of software from Manugistics Inc. is greatly appreciated.

APPENDIX

A1: Local flow

From Kaplan (1993), for a discrete time series, s_i ($i = 1, 2, \cdots, N$), we construct a time delay coordinate embedding based on an embedding dimension E, and a time delay L

$$\vec{x}_q = (s_q, s_{q+L}, \cdots, s_{q+L(E-1)}) \quad (1)$$

for $q = 1, 2, \cdots, N\text{-}L$. The embedding space is covered with a grid or mesh of 16^E cubes. The number of points in each cube j is n_j, and their time indices are $t_{j,k}$ where $k = 1, 2, \cdots, n_j$. For a given translation horizon, H, the change in state from time $t_{j,k}$ to $t_{j,k}+H$ for each of the n_j points in the cube j is

$$\Delta\vec{x}_{j,k} = \vec{x}(t_{j,k} + H) - \vec{x}(t_{j,k})$$

for $k = 1, 2, \ldots, n_j$. Since points near the edge of the cloud of points will have a directional bias towards the middle of the cloud, $\Delta x_{j,k}$ is mapped onto a sine function as

$$\Delta\tilde{x}_{j,k} = \left(\sin\left(2\pi\frac{x[t_{j,k}+H] - x[t_{j,k}]}{\lambda}\right), \sin\left(2\pi\frac{x[t_{j,k}+H+L] - x[t_{j,k}+L]}{\lambda}\right), \cdots, \sin\left(2\pi\frac{x[t_{j,k}+H+(E-1)L] - x[t_{j,k}+(E-1)L]}{\lambda}\right)\right),$$

where λ is a characteristic length of the embedded attractor; this sine mapping was not a feature of the original continuous implementation of this method (Kaplan and Glass 1992). In our computations, we have used the maximum amplitude of the time series as the value of λ.

An averaged vector, $|v_j|$, arises from cube j, where the number of vectors passing through the cube is n_j for $n \geq 2$. For different values of n and E these averaged vectors form a family of values L_n^E. These values are averaged over all values of n as

$$V = \left\langle \frac{(L_n^E)^2 - c_E^2/n}{1 - c_E^2/n} \right\rangle,$$

where $< >$ denotes average over all n. $c_E/n_j^{1/2}$ is the expectation value of L_n^E if the process were random. A more complete discussion of the derivation of c can be found in Kaplan and Glass (1992).

For the calculations presented in the text, we chose an embedding dimension $E = 4$, and mesh grain of 16^E cubes. Memory constraints became problematic when employing higher embedding dimensions with this method.

A2: Local dispersion

From Wayland et al. (1993), let x_q be defined as above, and let $x_1, \cdots, x_k$ be the k nearest neighbors of x_o, an arbitrary value of x_q. If we translate these nearest neighbors by a certain horizon, H, into the future, $y_0, \cdots, y_k$ are the k nearest "images" of the index point x_0 and its k nearest neighbors. The error, v, produced between the images and original points is

$$v_j = y_i - x_j.$$

The average error is

$$\langle v \rangle = \frac{1}{k+1}\sum_{j=0}^{k} v_j,$$

and the translation error is defined as

$$\epsilon_{trans} = \frac{1}{k+1}\sum_{j=0}^{k}\frac{\|v_j - \langle v\rangle\|^2}{\|\langle v\rangle\|^2},$$

where $\| \|$ indicates the length of the enclosed vector. ϵ_{trans} is essentially the variance of the errors v. N points are randomly chosen from the embedded attractor, and the median value of ϵ_{trans} is found.

For the calculations in the text, we chose a translation horizon, H, of 1, and 2% of the number of elements in the time series for the number of nearest neighbors, k.

A3: Nonlinear prediction

For an embedded time series, x, as above, again choose k nearest neighbors of a given index point x_0. The k nearest neighbors are translated by the

horizon, H, and their average translation is now

$$\langle v \rangle = \frac{1}{k} \sum_{j=1}^{k} x_{j+H},$$

which can be viewed as a zero-order (constant) prediction of the translation of x_0 by H time units.

The prediction error for the index point is

$$\epsilon_{\text{trans}} = |x_{0+H} - \langle v \rangle|,$$

and the error of predicting the mean of the time series is

$$\epsilon m_{\text{trans}} = |x_{0+H} - \text{mean}(x)|,$$

where $|\ |$ indicates absolute value.

The normalized prediction error, *NPE*, is

$$NPE = \frac{rms(\epsilon_{\text{trans}})}{rms(\epsilon m_{\text{trans}})}$$

where *rms* denotes root mean square.

For the calculations in the text, we chose an embedding dimension of 8, and 2% of the number of elements in the time series for the number of nearest neighbors, k.

A4: Autocorrelation

The autocorrelation (Box and Jenkins, 1976, Bendat and Piersol, 1986), $\Psi(L)$, is defined as

$$\Psi(L) = \frac{\sum_{i=1}^{n-L} (x_i - \langle x \rangle)(x_{i+L} - \langle x \rangle)}{\sum_{i=1}^{n-L} (x_i - \langle x \rangle)^2},$$

where L is the time delay and $\langle x \rangle$ denotes the mean value of x. The time series, after removal of the mean value, is shifted by a time lag, L, and the corresponding values of the shifted and original time series are multiplied and summed. These multiplications are normalized by the sum of the square of the error, $(x_i - \langle x \rangle)^2$. This is repeated for all time lags of interest, and a family of values, $\Psi(L)$, is generated.

A5: Hénon equations

The Hénon (1976) map is defined by the following equations

$$x_{n+1} = 1 - Ax_n^2 + y_n \qquad y_{n+1} = Bx_n.$$

In the simulations, we have used $A = 1.4$, and $B = 0.3$.

REFERENCES

Albano, A. M., J. Muench, C. Schwartz, A. I. Mees, and P. E. Rapp. 1988. Singular-value decomposition and the Grassberger-Procaccia algorithm. *Phys. Rev. A.* 38:3017–3026.

Basar, E. 1990. Chaotic dynamics, and resonance phenomena in brain function: progress, perspectives, and thoughts. *In* Chaos, and Brain Function. E. Basar (editor). Springer-Verlag, Berlin. 1–30.

Bendat, J. S., and A. G. Piersol. 1986. Random Data. John Wiley & Sons, New York. 566 pp.

Box, G. E. P., and G. M. Jenkins. 1976. Time series analysis, forecasting and control. Holden-Day, Oakland. 575 pp.

Broomhead, D. S., and G. P. King. 1986. Extracting qualitative dynamics from experimental data. *Physica D.* 20:217–236.

Chang, T., S. J. Schiff, and T. Sauer. 1994. Tests for deterministic chaos in noisy time series. *In* Proceedings of the Second Experimental Chaos Conference. W. Ditto, L. Pecora, M. Shlesinger, M. Spano, and S. Vohra (editors). World Scientific, Singapore. In press.

Ditto, W. L., S. N. Rauseo, and M. L. Spano. 1990. Experimental control of chaos. *Phys. Rev. Lett.* 65:3211–3214.

Farmer, J. D., and J. J. Sidorowich. 1988. Exploiting chaos to predict the future and reduce noise. *In* Evolution, Learning and Cognition. Y. C. Lee (editor). World Scientific, Singapore. 279–330.

Garfinkel, A., M. Spano, W. L. Ditto, and J. Weiss. 1992. Controlling cardiac chaos. *Science.* 257:1230–1235.

Gossard, J.-P., M. K. Floeter, T. Chang, S. J. Schiff, and R. E. Burke. 1994. Fluctuations of excitability in the monosynaptic reflex pathway to lumbar motoneurons in the cat. *J. Neurophysiol.* In press.

Grillner, S. 1981. Control of locomotion in bipeds, tetrapods, and fish. *In* Handbook of Physiology. Sec. 1: The Nervous System. Vol 2. Motor Control. Part 2. V. B. Brooks (editor). American Physiological Society, Bethesda, MD. 1179–1236.

Henon, M. A. 1976. Two dimensional mapping with a strange attractor. *Comm. Math. Phys.* 50:69–77.

Hunt, E. 1991. Stabilizing high-period orbits in a chaotic system: the diode resonator. *Phys. Rev. Lett.* 67:1953–1955.

Kaplan, D. T. 1993. Evaluating deterministic structure in maps deduced from discrete-time measurements. *Int. J. Bifurcations and Chaos.* In press.

Kaplan, D. T., and L. Glass. 1992. Direct test for determinism in a time series. *Phys. Rev. Lett.* 68:427–430.

Kaplan, D. T., and L. Glass. 1993. Coarse-grained embeddings of time series: random walks, Gaussian random processes, and deterministic chaos. *Physica D.* 64:431–454.

King, C. C. 1991. Fractal and chaotic dynamics in nervous systems. *Progr. Neurobiol.* 36:279–308.

Kostelich, E. J., and J. A. Yorke. 1990. Noise reduction: finding the simplest dynamical system consistent with the data. *Physica D.* 41:183–196.

Lloyd, D. P. C., and V. J. Wilson. 1957. Reflex depression in rhythmically active monosynaptic reflex pathways. *J. Gen. Physiol.* 40:409–434.

May, R. M. 1976. Simple mathematical models with very complicated dynamics. *Nature.* 261:459–467.

Molt, J. T., and E. L. Gasteiger. 1976. Variability in spinal reflexes: a correlation with spontaneous slow wave activity in cat spinal cord. *Exp. Neurol.* 52:132–145.

Moon, F. C. 1992. Chaotic and Fractal Dynamics. John Wiley & Sons, New York. 508 pp.

Ott, E. 1993. Chaos in Dynamical Systems. Cambridge University Press, Cambridge, England. 385 pp.

Ott, E., C. Grebogi, and J. A. Yorke. 1990. Controlling chaos. *Phys. Rev. Lett.* 64:1196–1199.

Packard, N. H., J. P. Crutchfield, J. D. Farmer, and R. S. Shaw. 1980. Geometry from a time series. *Phys. Rev. Lett.* 45:712–716.

Rall, W. 1955. Experimental monosynaptic input-output relations in the mammalian spinal cord. *J. Cell Comp. Physiol.* 46:413–437.

Rall, W., and C. C. Hunt. 1956. Analysis of reflex variability in terms of partially correlated excitability fluctuations in a population of motoneurons. *J. Gen. Physiol.* 39:397–442.

Redman, S., and B. Walmsley. 1983. Amplitude fluctuations in synaptic potentials evoked in cat spinal motoneurones at identified group Ia synapses. *J. Physiol. (Lond.)* 343:135–145.

Rivera, A. D. C., T. Burke, S. J. Schiff, and I. P. Weiss. 1994. An experimental study of reflex variability in selective dorsal rhizotomy. *J. Neurosurg.* In press.

Roy, R., T. W. Murphy, T. D. Maier, and Z. Gills. 1992. Dynamical control of a chaotic laser: experimental stabilization of a globally coupled system. *Phys. Rev. Lett.* 68:1259–1262.

Rudomin, P., R. E. Burke, R. Nunez, J. Madrid, and H. Dutton. 1975. Control by presynaptic correlation: a mechanism affecting information transmission from Ia fibers to motoneurons. *J. Neurophysiol.* 38:267–289.

Rudomin, P., and H. Dutton. 1969. Effects of conditioning afferent volleys on variability of monosynaptic responses of extensor motoneurons. *J. Neurophysiol.* 32:140–157.

Sauer, T. 1992. A noise reduction method for signals from nonlinear systems. *Physica D.* 58:193–201.

Sauer, T. 1993. Time series prediction using delay coordinate embedding. *In* Time Series Prediction: Forecasting the Future and Understanding the Past. A. S. Weigend and N. A. Gershenfeld (editors). SFI Studies in the Sciences of Complexity. Vol 15. Addison-Wesley, Reading, MA. 175–193.

Sauer, T., J. Yorke, and M. Casdagli. 1991. Embedology. *J. Stat. Phys.* 65:579–616.

Schiff, S. J. 1992. Resolving time-series structure with a controlled wavelet transform. *Optical Engineering.* 31:2492–2495.

Schiff, S. J., and T. Chang. 1992. Differentiation of linearly correlated noise from chaos in a biologic system using surrogate data. *Biol. Cybern.* 67: 387–393.

Schiff, S. J., T. Sauer, and T. Chang. 1994. Discriminating deterministic versus stochastic dynamics in neuronal activity. *Integrative Physiol. Behav. Sci.* In press.

Sherrington, C. S. 1906. The Integrative Action of the Nervous System. Charles Scribner's Sons, New York. 433 pp.

Shinbrot, T., C. Grebogi, E. Ott, and J. A. Yorke. 1993. Using small perturbations to control chaos. *Nature.* 363:411–417.

Solodkin, M., I. Jimenez, W. F. Collins, L. M. Mendell, and P. Rudomin. 1991. Interaction of baseline synaptic noise and Ia EPSPs: evidence for appreciable negative correlation under physiological conditions. *J. Neurophysiol.* 65:928–945.

Sugihara, G., and R. M. May. 1990. Nonlinear forecasting as a way of distinguishing chaos from measurement error in time series. *Nature.* 344: 734–741.

Takens, F. 1981. Detecting strange attractors in turbulence. *Lecture Notes in Mathematics.* 898:366–381.

Theiler, J., S. Eubank, A. Longtin, B. Galdrikian, and J. D. Farmer. 1992. Testing for nonlinearity in time series: the method of surrogate data. *Physica D.* 58:77–94.

Theiler, J., P. Linsay, and D. M. Rubin. 1993. Detecting nonlinearity in data with long coherence times. *In* Time Series Prediction: Forecasting the Future and Understanding the Past. A. S. Weigend and N. A. Gershenfeld (editors). SFI Studies in the Sciences of Complexity. Vol. 15. Addison-Wesley, Reading, MA. 430–455.

Wayland, R., D. Bromley, D. Pickett, and A. Passemante. 1993. Recognizing determinism in a time series. *Phys. Rev. Lett.* 70:580–582.

Weiss, I. P., and S. J. Schiff. 1993. Reflex variability in selective dorsal rhizotomy. *J. Neurosurg.* 79:346–353.

Whitney, H. 1936. Differentiable manifolds. *Ann. Math.* 37:645–680.